Appl. Phys. B 85, 445–452 (2006)
DOI: 10.1007/s00340-006-2365-0

Applied Physics B
Lasers and Optics

M.R. MCCURDY[1,2]
Y.A. BAKHIRKIN[1]
F.K. TITTEL[1,✉]

Quantum cascade laser-based integrated cavity output spectroscopy of exhaled nitric oxide

[1] Rice Quantum Institute, Rice University, 6100 Main St., Houston, TX 77005, USA
[2] Medical Scientist Training Program, Baylor College of Medicine, 1 Baylor Plaza, Houston, TX 77030, USA

Received: 9 May 2006/Revised version: 16 June 2006
Published online: 18 July 2006 •

ABSTRACT A nitric oxide (NO) sensor employing a thermoelectrically cooled, continuous-wave, distributed feedback quantum cascade laser operating at 5.47 μm (1828 cm^{-1}) and off-axis integrated cavity output spectroscopy was used to measure NO concentrations in exhaled breath. A minimum measurable concentration (3σ) of 3.6 parts-per-billion by volume (ppbv) of NO with a data-acquisition time of 4 s was demonstrated. Five prepared gas mixtures and 15 exhaled breath samples were measured with both the NO sensor and for intercomparison with a chemiluminescence-based NO analyzer and were found to be in agreement within 0.6 ppbv. Exhaled NO flow-independent parameters, which may provide diagnostic and therapeutic information in respiratory diseases where single-breath measurements are equivocal, were estimated from end-tidal NO concentration measurements collected at various flow rates. The results of this work indicate that a laser-based exhaled NO sensor can be used to measure exhaled nitric oxide at a range of exhalation flow rates to determine flow-independent parameters in human clinical trials.

PACS 07.07.Df; 33.20.Ea; 42.62.Fi; 87.80.-y

1 Introduction

Exhaled nitric oxide (eNO) is an important biomarker in many respiratory diseases. eNO levels have been extensively studied in asthma and may be incorporated into clinical care in the near future [1, 2]. These measurements may be clinically useful in other chronic respiratory conditions, such as chronic obstructive pulmonary disease, particularly if the NO contributions are partitioned into alveolar and conducting airway regions [3, 4].

eNO levels generally range over 4–15 ppbv in healthy human subjects and 10–160 ppbv in subjects with untreated asthma when breath is collected at the standard 3 l/min, in accordance with the American Thoracic Society (ATS) recommendations. The ATS recommends that an eNO analyzer has a sensitivity < 1 ppbv (< 0.5 ppbv noise), a response time of 0.5 ms, a range of 1–500 ppbv, and a reproducibility better than 1 ppbv [5].

Inflammation in chronic obstructive pulmonary disease (COPD) occurs predominantly in the alveolar region (where an O_2/CO_2 exchange occurs), as compared to inflammation in asthma that occurs more in the conducting airways. Single-breath measurements at a constant flow rate are adequate for monitoring conducting airway inflammation in asthma but cannot differentiate the quantity of nitric oxide arising from the alveoli and the conducting airway. A model of the lung was developed by partitioning the lung into two compartments – a conducting airway with an NO diffusing barrier and an alveolar region [6]. Three parameters – the fraction of alveolar NO (F_aNO), the fraction of NO in the airway wall tissue (F_wNO), and the rate of NO transferred from the airway wall (airway NO diffusing capacity, D_wNO) – describe the NO excretion from the lung using this model. F_aNO, which is NO arising from the alveoli and respiratory bronchioles, may be a better estimate of peripheral lung inflammation and therefore may be a better marker of inflammatory status than a single-breath NO level in COPD [3, 4]. Additionally, D_wNO may be elevated in a subset of COPD patients and aid in the choice of therapy. To estimate the three flow-independent parameters, two techniques have been described. A single exhalation can be used with a varying flow rate during exhalation, requiring fast time-resolved measurements. Alternatively, the plateau NO concentration (NO level at the end of an exhalation) can be measured during repeated single-breath measurements, and algorithms can be used to estimate the three parameters.

Presently, exhaled nitric oxide is measured in the clinical research setting using an ozone-based chemiluminescence technique that is approved by the US Food and Drug Administration (FDA) to monitor inflammation in asthma. This method takes advantage of the generation of light from the reaction of NO with ozone (O_3) and is sensitive to quenching by both carbon dioxide and water [7, 8]. The chemiluminescence analyzers in the market today exhibit the required sensitivity for exhaled NO measurements and have opened the door to clinical exhaled NO research. However, there are several issues concerning requirements for frequent calibration and technical maintenance, the generation and destruction

✉ Fax: +1-713-348-4833, E-mail: fkt@rice.edu

of ozone, and high voltage. Differences in measured values between chemiluminescence analyzers have been reported, and a major contributing factor may be due to differences in calibration gases and procedures [9, 10]. Addressing these issues with alternative laser-based instrumentation technologies may facilitate the acceptance of exhaled NO measurement methods in general routine health care, especially when moving into patient home monitoring.

Various non-optical and optical techniques for nitric oxide measurement have been reported. A compact NO sensor based on electrochemical sensor technology, reported by Hemmingsson et al. [11], achieved a sensitivity of 3 ppbv in reference-gas tests and a response time of 15 s. Background-free Faraday-modulation spectroscopy was reported to measure nitric oxide with a sensitivity of a few parts per billion by volume (ppbv) [12]. Laser spectroscopy allows sensitive, selective, and fast-response NO concentration measurements. Lead salt laser-based systems have achieved 1.5 ppbv and better and are commercially available [13]. A quantum cascade laser (QCL) spectrometer using a multipass cell has achieved a sensitivity of < 0.1 ppbv [14]. The cavity ring-down spectroscopy (CRDS) technique uses ultra-high-reflectivity mirrors ($R > 99.99\%$) to reach noise-equivalent sensitivity at the sub-ppbv level in several seconds using a comparatively small sample volume [15]. In the case of integrated cavity output spectroscopy (ICOS), the spectral output from a cavity resonator is time averaged. Several ICOS-based NO detection systems have been reported [16–19]. A practical advantage of ICOS is the high achievable detection sensitivity in a relatively small sample volume. A distributed feedback (DFB), continuous-wave (cw) QCL is an ideal spectroscopic source for ICOS-based sensor platforms for real-world applications because of its narrow laser spectral width (≤ 3 MHz [19]), necessary for efficient laser cavity coupling, and high power (> 0.1 W).

In this work we used a novel thermoelectrically cooled (TEC), cw, DFB QCL from Alpes operating at 1828 cm^{-1} with 31-mW maximum power [20]. The basic sensor platform is an off-axis ICOS configuration with a 50-cm-long optical cavity and is a slightly modified version of our previously reported work [19]. The sensor was compared to the commonly used Sievers nitric oxide analyzer (model 280). Furthermore, flow-independent parameters were calculated.

2 Sensor architecture and experimental method

2.1 *Sensor architecture*

A schematic of the ICOS sensor is depicted in Fig. 1. A similar platform has been described previously [19], and only the salient features and differences are described here. A TEC cw DFB QCL, operating at 5.47 μm, was installed in a compact evacuated housing. The housing was equipped with a 25-mm-diameter CaF_2 window and a single-stage thermoelectric cooler (Melcor Corporation, type UT8-12-40F1) that provides thermal control of the QCL's mount. A 25-mm-diameter ZnSe aspherical lens, with an antireflection coating and 12.7-mm effective focal length, collimates and directs the QCL beam into the ICOS cavity. The optical ICOS cavity is formed by two highly reflective 50.8-mm-diameter concave mirrors (1-m radius of curvature) separated by a 50-cm stainless steel spacer. The high-reflectivity (low-loss) dielectric ICOS mirrors used in this work were employed previously [18, 19]. The expected absorbance in the HITRAN-2000 database [21] was compared to the measured absorbance to estimate the effective path length to be ~ 500 m assuming that the measured absorption is linear at low ($<$ 100 ppbv) NO concentrations [22]. The cavity was aligned off-axis with respect to the laser beam, providing improved cavity mode noise suppression, which is the critical factor determining the sensitivity of the ICOS technique [18, 22]. The cavity length was dithered using an assembly consisting of three piezo-electric actuators attached to one of the resonator mirrors (see Fig. 1), which enhanced the signal-to-noise ratio (SNR) by a factor of ~ 5. Further suppression of cavity mode noise, leading to enhanced sensitivity, was achieved by averaging the cavity resonances. The PZT-activated ICOS mirror oscillated at a frequency of ~ 183 Hz with a maximum translation of ~ 15 μm, which covers several free spectral ranges of the cavity. The dither frequency was chosen to avoid an integer multiple of the scan rate of 1 kHz.

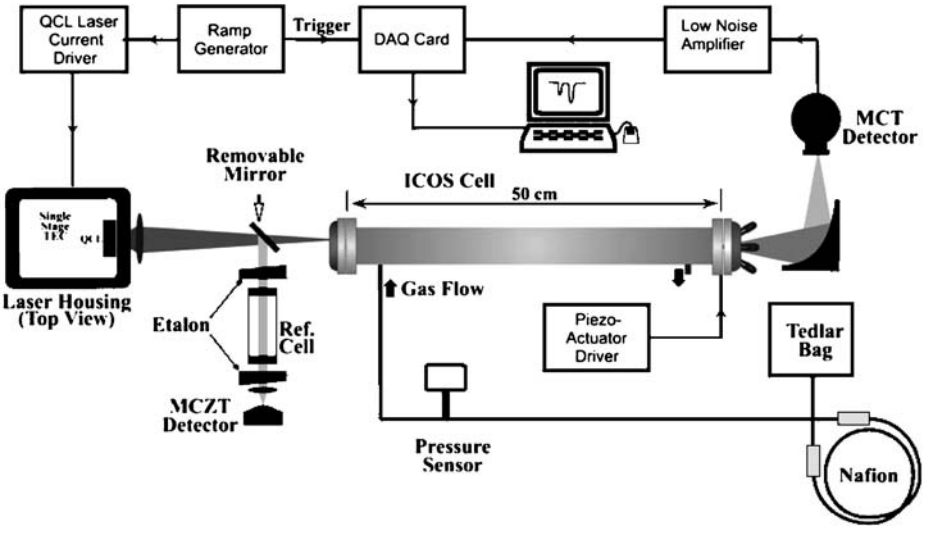

FIGURE 1 Thermoelectrically cooled cw, DFB, QCL-based off-axis ICOS sensor. MCT is a cryogenically cooled photovoltaic HgCdTe detector and MCZT is a thermoelectrically cooled HgCdZnTe photodetector

2.2 *Operating characteristics of the quantum cascade laser source*

The laser was a junction up-mounted DFB laser, which operated at a temperature range from 0 °C to −40 °C with a total tuning range from 1822 cm^{-1} to 1832.5 cm^{-1}, according to the manufacturer (Alpes Lasers, Switzerland). The spectral output, current and temperature tuning ranges, and tuning rates of the QCL were evaluated using a 10-cm reference cell filled with a NO:N_2 calibration mixture, an air-spaced Fabry–Pérot etalon consisting of two wedged ZnSe windows, and the HITRAN-2000 database [21]. The temperature and current tuning rates were found to be $\sim -0.17\,cm^{-1}/K$ and $\sim -0.019\,cm^{-1}/K$, accordingly. A temperature controller (Wavelength Electronics, Inc., model MPT-10000) provides a long-term temperature stability δT of ≤ 0.01 °C, limiting the spectral line shift to $\leq 0.002\,cm^{-1}$, which is negligible compared to the NO line width at 100 Torr ($0.020\,cm^{-1}$). At a fixed temperature of the laser thermal sink, the frequency of the output radiation can be tuned by varying the QCL current. A current driver (ILX Lightwave, model LDX-3232) was used to operate the QCL. The measured laser radiation power after the ZnSe aspherical lens at −24 °C is plotted in Fig. 2 as a function of the QCL drive current and corresponding wavenumber. A threshold of 244 mA and a slope efficiency of $\sim$ 128 mW/A were observed.

A simulated spectrum of typical exhaled molecules in the tuning range of the QCL using the HITRAN-2000 database is shown in the upper plot of Fig. 3. The lower plot of Fig. 3 depicts the tuning range achieved with the current ramp used in this work. The concentrations of NO (20 ppbv), CO_2 (4%), and NH_3 (300 ppbv) represent typical exhaled breath concentrations for a non-smoker with chronic obstructive pulmonary disease who has no other diseases or comorbidities. Because of a strong interference of H_2O in the tuning range of the laser, H_2O was selectively removed from the breath samples before entering the sample cell for concentration measurement. The H_2O concentration is reduced from 2.5% to $\sim$ 500 ppm using a commercially available Nafion dryer (Perma Pure, model PD-50T, 72-in length) with a sample flow of 0.1 l/min and a N_2 counterflow of 0.5 l/min (shown in Fig. 1). The combined NO absorption line $P_{1/2}$ (13.5), which is a superposition of two lambda coupling components centered at 1828.06 cm^{-1}, was selected for concentration measurements as it is the most intense line free from H_2O interference in the QCL tuning range. A QCL mount temperature of −24 °C and a ramp of 0.24–0.28 A were chosen to optimize absorption measurement of the $P_{1/2}$ (13.5) NO line. Three water lines were utilized for frequency calibration.

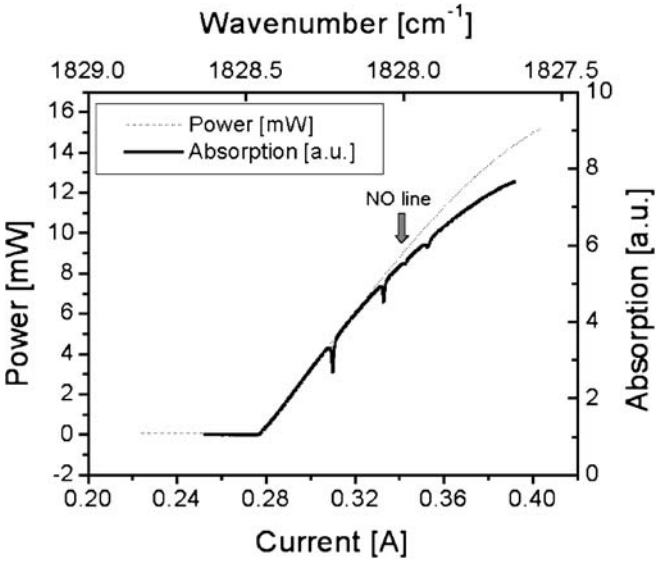

FIGURE 2 Power dependence of QCL at 1828 cm^{-1} on drive current at a laser submount temperature of −24 °C. The QCL power was measured in front of the ICOS cavity. The *block arrow* represents the required QCL driver current (342 mA) to obtain the selected NO line at 1828.06 cm^{-1}. An *absorption curve* at the corresponding driver current and wavelength is overlaid to show the positions of the three water lines and the NO line

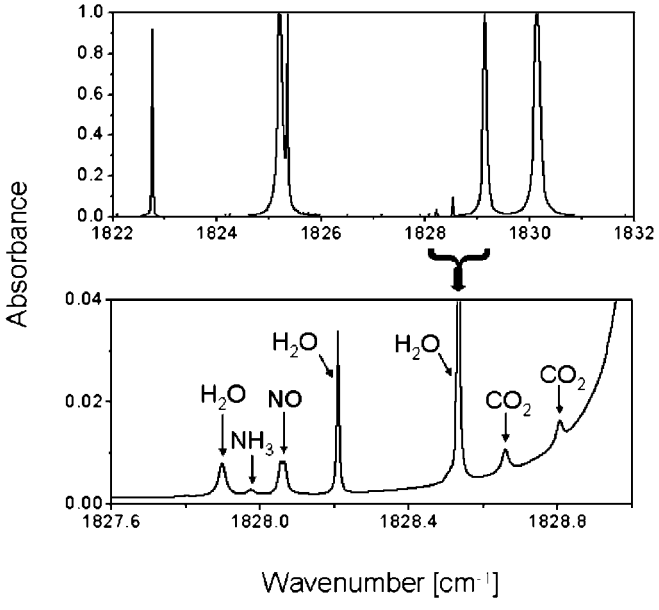

FIGURE 3 Simulated spectrum (HITRAN 2000). The *upper plot* shows a spectrum of molecules present in exhaled breath in the tuning range of the QCL at 1828 cm^{-1}. The *lower plot* shows the spectral region acquired by each scan. The absorption feature at 1828.06 cm^{-1} was used for NO concentration measurements. The following parameters were used for the simulation: optical path length − 500 m, pressure − 100 Torr, NO − 20 ppbv, H_2O (after Nafion filter) − 100 ppm, CO_2 − 4%, NH_3 − 300 ppbv

2.3 *Single-breath collection*

A custom-built breath-collection device was used to collect single breaths into Tedlar bags with the subject exhaling at specific constant flow rates (Fig. 4). The device is a modified version of a single breath collection system [23]. The modified collection system makes use of a two-way non-rebreathing valve and filter to remove NO from inspired air and a larger-diameter tube on the exhalation port to allow exhalation at higher flow rates (up to 15 l/min). Exhaled nitric oxide has a marked dependence on flow rate. The American Thoracic Society (ATS) published recommendations for single-breath collection in adults and children [1]. The most notable recommendations are: (a) providing a back pressure > 6 Torr to prevent nasal contamination and (b) maintaining a constant exhalation flow at a standardized flow rate. Mouth pressure was maintained by an adjustable stopcock valve and was monitored with a pressure sensor (model 860, Autotran, Eden Prairie, MN). A constant exhalation flow rate was main-

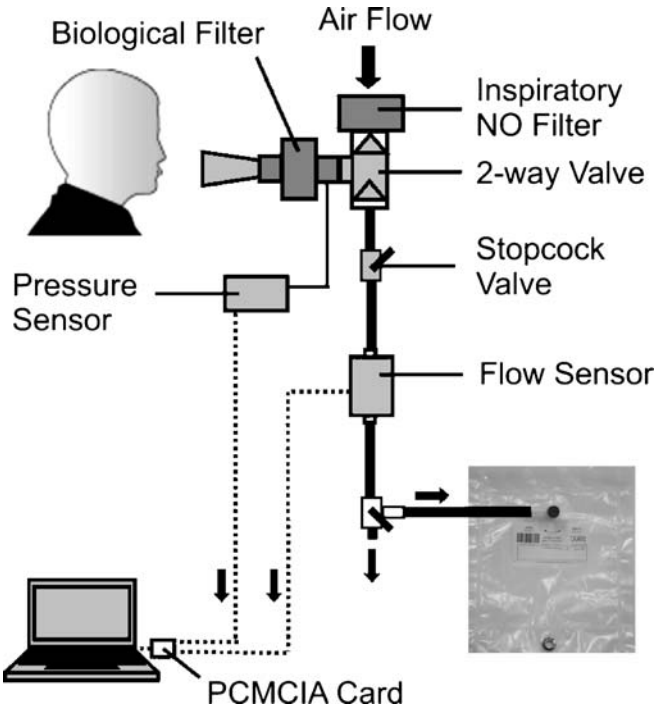

FIGURE 4 Breath-collection device. The subject inhales deeply and exhales through a mouthpiece. Pressure and flow are measured with in-line sensors. An adjustable stopcock valve provides resistance to flow to prevent nasal contamination. Exhaled air is collected in a Tedlar bag after the initial portion of the breath is discarded

tained using feedback from an in-line mass flowmeter (model 4021, TSI Inc., Shoreview, MN) displayed on a laptop personal computer (PC) using a Labview (National Instruments, Austin, TX) interface.

Breath was collected at various constant flow rates from each subject to estimate the flow-independent parameters (described in Sect. 2.4, below). Resistance from the stopcock valve was adjusted between flow-rate sessions to maintain a mouth pressure in the range of 8 to 15 cm H_2O. Because the NO level in breath reaches a plateau level during a single breath at constant flow [24], the second portion of the exhaled breath was collected by discarding the first portion of the breath into ambient air, based on exhalation time to reach the NO plateau. The exhalation time of discarded breath varied depending on the flow rate: for 10 ml/s, breath was collected after 15 s; for 50 ml/s, 12 s; for 100 ml/s, 9 s; for 200 ml/s, 6 s; and for 260 ml/s, 5 s. After the appropriate elapsed time, a three-way valve diverted exhaled air into a Tedlar bag for the remainder of the exhalation. Single-breath collections were repeated until the Tedlar bag reached $\sim 80\%$ capacity. Using this method, the plateau region of each exhaled breath was collected, and the measured NO values represent the NO plateau concentration. The Tedlar bags were measured within 12 h of breath collection. Preliminary results indicate that the NO level is stable for 24 h in the Tedlar bags.

2.4 *Estimation of flow-independent parameters*

A two-compartment model of the lung was developed to adequately represent the marked dependence of eNO on exhalation flow [25]. Three flow-independent NO exchange parameters can describe the airway compartment: the alveolar region concentration ($C_A NO$), the airway NO diffusing capacity ($D_w NO$), and the maximum airway wall NO flux or airway wall NO concentration ($F_w NO$). Several techniques have been described to estimate the flow-independent parameters (see [5]).

For this work, a modified method based on that used by Hogman et al. was utilized [26]. Only the salient features are presented here. The alveolar component of exhaled NO output is estimated based on a model of the lung. The model comprises an alveolar compartment and a conducting airway compartment modeled as a cylindrical tube of constant radius with a diffusion barrier layer between the tissue and the airway. Based on this model, the following equation can be derived for the exhaled NO concentration as a function of the flow rate ($\dot{Q}$) [26]:

$$\mathrm{FeNO} = \mathrm{F_wNO} - (\mathrm{F_wNO} - \mathrm{F_aNO}) \times \mathrm{e}^{-\mathrm{D_wNO}/\dot{Q}}\,, \tag{1}$$

where $F_e NO$ is the fractional excretion of NO as a function of flow rate, $F_w NO$ is the fraction of NO in the airway wall tissue, $F_a NO$ is the fraction of alveolar NO, and $D_w NO$ is the rate of NO transferred from the airway wall. The NO output ($\dot{V}_e NO$) can be utilized as suggested in [25] to obtain

$$\dot{V}_\mathrm{e}\mathrm{NO} = \dot{Q} \times \left(\mathrm{F_wNO} - (\mathrm{F_wNO} - \mathrm{F_aNO}) \times \mathrm{e}^{-\mathrm{D_wNO}/\dot{Q}}\right)\,. \tag{2}$$

At high exhalation flows, when $\dot{Q} \gg \mathrm{D_wNO}$, the exponential function can be linearly approximated as $1 - \mathrm{D_wNO}/\dot{Q}$. After mathematical manipulation, (3) is obtained:

$$\dot{V}_\mathrm{e}\mathrm{NO} = \mathrm{F_eNO} \times \dot{Q} \times (\mathrm{F_wNO} - \mathrm{F_aNO}) \times \mathrm{D_wNO} + \mathrm{F_aNO} \times \dot{Q}\,. \tag{3}$$

Equation (3) is a line with a slope (S):

$$\mathrm{S} = \mathrm{F_aNO}\,. \tag{4}$$

The intercept (I) of (3) can be found, by setting $\dot{Q} = 0$, to be

$$\mathrm{I} = (\mathrm{F_wNO} - \mathrm{F_aNO}) \times \mathrm{D_wNO}\,. \tag{5}$$

In this method, the flow-independent parameters – $F_a NO$, $F_w NO$, and $D_w NO$ – are obtained from three flow rates; one very low (0.5 l/min), a medium flow rate (3 l/min), and a high flow rate (15 l/min). To determine $F_a NO$, the NO elimination (the product of plateau NO and exhalation flow rate) versus exhalation flow rate was plotted using the medium- and high-flow rates, and a line was regressed to determine the slope ($F_a NO$). Next, $D_w NO$ and $F_w NO$ were determined from the low- and medium-flow NO concentrations using an iterative algorithm that uses (1), (4), and (5). Details are given in the appendix.

2.5 *Intercomparison of QCL-based ICOS sensor with a commercial NO analyzer*

The ICOS-based sensor was compared to a Sievers nitric oxide analyzer (NOA) model 280 (Sievers, Inc., Boulder, CO), which utilizes the chemiluminescence technique. Twenty samples from 1-l Tedlar bags were analyzed

by both instruments – 15 breath samples and five prepared gas mixtures. The gas mixtures were 100%, 75%, 50%, 25%, and 5% of a calibration gas mixture (77-ppbv NO:N_2, prepared by Scott Specialty Gases, Inc.) diluted in ultra-pure N_2 gas (Matheson Tri-Gas). The exhaled breath samples were collected at various flow rates from healthy volunteers and patients with chronic obstructive pulmonary disease. Each Tedlar bag was measured by both instruments within 12 h. Written informed consent was obtained by all subjects and the protocol was approved by the Rice University and Baylor College of Medicine Institutional Review Boards.

The Sievers NOA was calibrated according to the manufacturer's instructions using an NO-free gas (< 0.1 ppbv NO) and a 40-ppmv NO gas mixture. Additionally, multiple calibrations were performed using the NO-free gas prior to NO concentration measurements. Results of the intercomparison were analyzed according to the method of Bland and Altman for comparing agreement between two clinical measurement methods [27].

3 NO sensor results

3.1 *ICOS sensor performance*

The calibration mixture of 77-ppbv NO:N_2 mentioned in Sect. 2.5 was used for the performance evaluation of the QCL-based NO sensor system. A custom gas mixer, consisting of two mass-flow controllers (MKS model 1179A) feeding into a common chamber, was used to obtain reduced NO concentration levels. A gas-flow system described in detail in [17] was utilized for such measurements.

The gain factor $G = R/(1-R)$ is ~ 4000 for the pair of ICOS cavity mirrors with a reflectivity R of $\sim 99.975\%$ at 5.47 μm (1828 cm^{-1}) [17]. In order to ensure that the cavity provides linear gain, the condition $GA \ll 1$ should be satisfied, where A is the single-pass absorption. For the maximum NO concentration of 77 ppbv the factor GA is ~ 0.16. This result verifies that for a smaller NO concentration the amplitude of the absorption signal scales linearly with concentration values.

NO concentration measurements were made with the 50-cm-long ICOS cell by applying a QCL current ramp across the absorption line with a frequency of 1 kHz. The cavity output signal was sampled, averaged, and processed using a fast data-acquisition card and a PC. The results, using the QCL operating at 1828 cm^{-1} described in Sect. 2.2, are depicted in Fig. 5. The blue curve shows a 77-ppbv NO absorption line obtained from averaged ICOS signals. The NO absorption line at 1828.06 cm^{-1} (as was mentioned in Sect. 2.2) is a superposition of two lambda coupling components of the P branch centered at 1828.06 cm^{-1} with a spectral assignment of $P_{1/2}$ (13.5). The red line represents a Voigt fitted curve. Spectra were collected by ramping the laser current at 1000 Hz to cover the spectral region of interest and collecting the detector output using a data-acquisition system (PCI-6111, National Instruments) connected to the PC and controlled by LabView software. The sampling rate for the digitizer was 5 Msample/s. Thus, each scan consisted of approximately 5000 data points (≈ 4000 points per spectral feature). By beginning the current scans below the threshold for lasing, a 'zero' laser level for the AC-coupled detector signal could be established. Typically, 10 000 spectral scans (for a total measurement time of ~ 4 s) were averaged for each NO determination. The minimum detectable concentration (3σ) was estimated to be 3.6 ppbv based on the standard deviation of the Voigt fit residual.

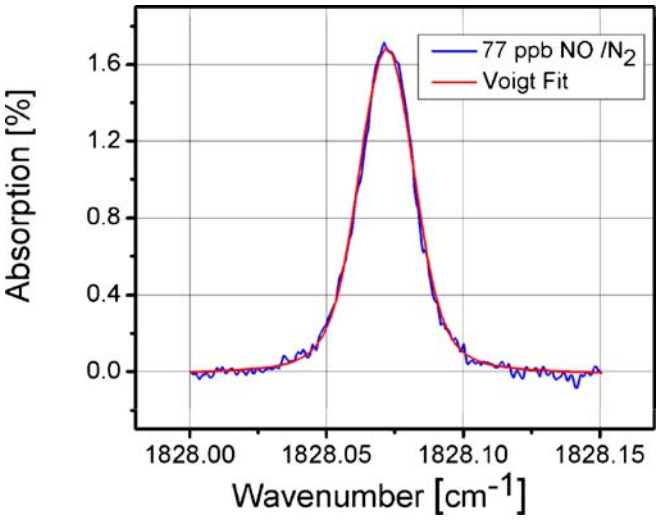

FIGURE 5 NO absorption feature at 1828.06 cm^{-1} of a calibration mixture of 77 ppbv NO in N_2 as a balance gas. A minimum detectable concentration of 3.6 ppbv (3σ) was determined from the residual of a Voigt fit with a 4-s data-acquisition time

3.2 *Estimation of flow-independent parameters*

Plateau NO was measured at five constant exhalation flow rates from a patient with severe chronic obstructive pulmonary disease. Four flow rates > 40 ml/min were used to verify the linearity of NO elimination rate versus exhalation flow rate for higher flow rates. Figure 6 shows the NO absorption feature at 1828.06 cm^{-1} for the calibration mixture (77 ppbv), 10 ml/s (58.5 ppbv), 50 ml/min

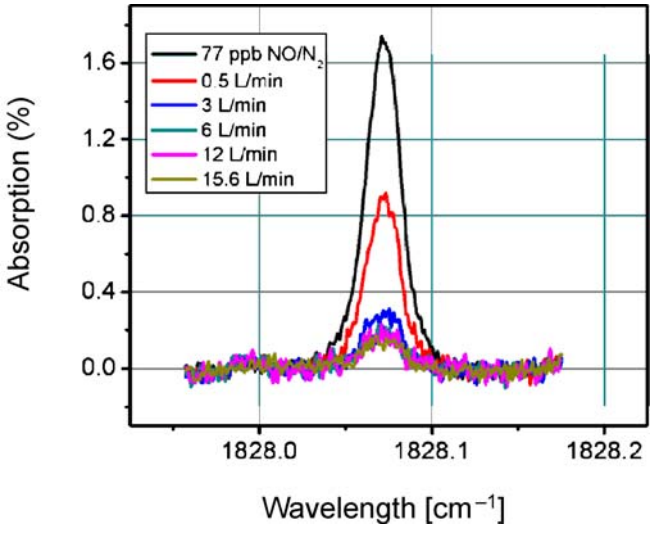

FIGURE 6 Exhaled NO data from a patient with chronic obstructive pulmonary disease. Exhaled breath was collected in the region of the NO plateau at various flow rates, and NO was subsequently measured using off-axis ICOS with a QCL operating at 1828.06 cm^{-1}

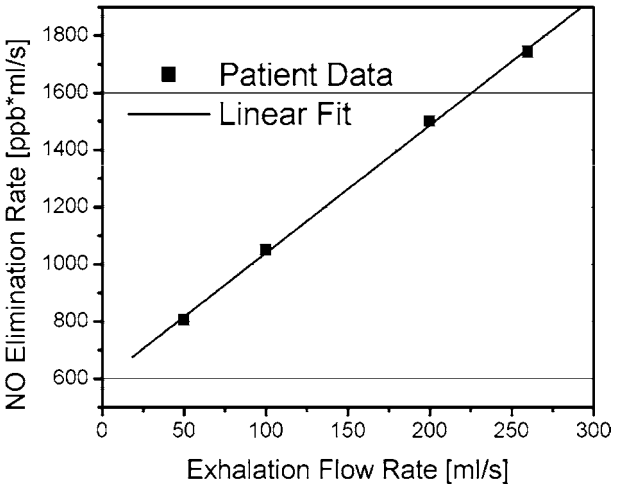

FIGURE 7 Plot of NO elimination rate (Vno, the product of the plateau NO concentration and the exhalation flow rate) versus exhalation flow rate (Ve) for exhalation flows greater than 40 ml/s. The slope of the regressed line, 4.6, is an estimate of the fraction of alveolar NO (CaNO) in ppbv

(16.1 ppbv), 100 ml/min (10.5 ppbv), 200 ml/min (7.5 ppbv), and 260 ml/min (6.7 ppbv). The NO elimination rate (the product of plateau NO concentration and exhalation flow rate) versus flow rate was plotted for the four flow rates > 40 ml/min to determine CaNO from the slope of the regressed line and this was determined to be 4.6 ppbv (Fig. 7). The other flow-independent parameters were determined, as described in the appendix, to be $D_wNO = 2.7$ ml/s and $F_wNO = 87.6$ ppbv. These values are similar to reported values in severe chronic obstructive pulmonary disease [3, 4, 26].

3.3 *Intercomparison of ICOS sensor and Sievers nitric oxide analyzer*

Five prepared gas mixtures and 15 breath samples were measured with each instrument. The Pearson correlation coefficient was used to determine the correlation between the values for plateau NO determined by the two methods (Fig. 8). The ICOS sensor and Sievers NOA showed significant correlation among the 20 samples ($r^2 = 0.992$). The agreements, calculated using the method described by Bland and Altman, between the ICOS sensor and the Sievers NOA (Fig. 9) had a mean proportional difference of 0.55 ppbv and 95% limits of agreement of −3.3 ppbv and 4.3 ppbv.

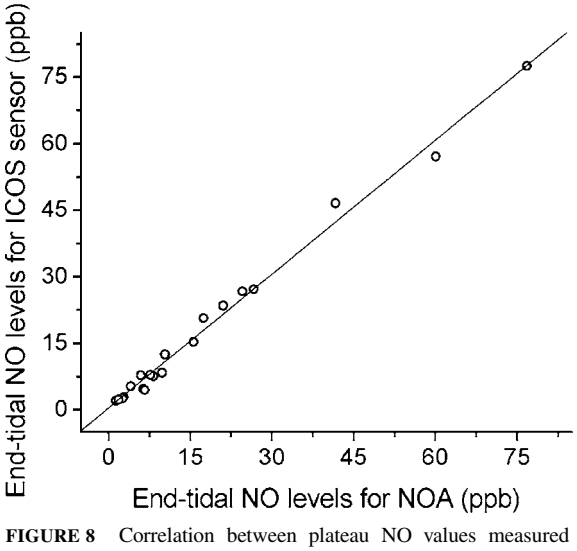

FIGURE 8 Correlation between plateau NO values measured with the ICOS sensor and a Sievers nitric oxide analyzer (NOA) chemiluminescence instrument ($r^2 = 0.992$, slope = 1.01)

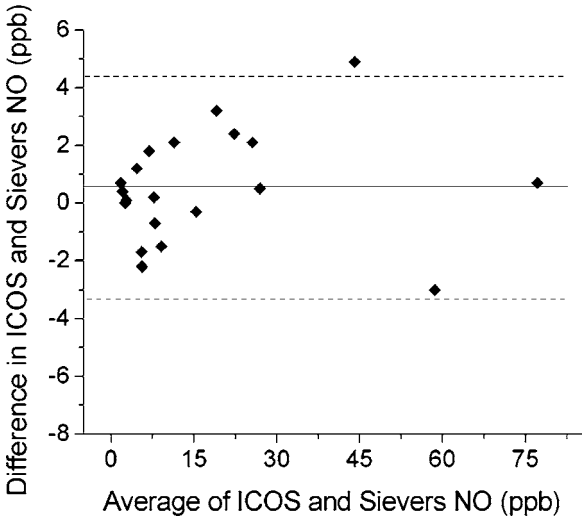

FIGURE 9 Bland and Altman plot for 15 breath samples and five prepared samples. For breath samples, plateau NO was collected at various flow rates from multiple patients with chronic obstructive pulmonary disease. *Solid line* = mean difference between values obtained using the two methods (0.55 ppbv); *dashed lines* represent the limits of agreement, −4.34 ppbv and 3.25 ppbv (±2 SD)

4 Discussion

The main finding of this study has been the demonstration of performing sensitive and selective NO concentration measurements at the ppbv level with a QCL-based ICOS gas sensor. These measurements are in agreement with a Sievers NOA. The chemiluminescence technique can be considered the gold standard. Since the true plateau NO concentration in each sample was not known, the degree of agreement between the two techniques was assessed. The mean plateau NO difference between the two methods is an estimate of the bias of one method relative to the other [28]. The mean difference suggests that a plateau NO value measured by the ICOS sensor, on average, is 0.55 ppbv lower than the Sievers NOA. The limits of agreement denote that the difference between the ICOS sensor and the Sievers NOA will be between −4.34 ppbv and 3.25 ppbv for 95% of the measurements. These results suggest that published findings of NO measurements from the two instruments are in agreement and that the trends (i.e. differences between patient groups) will agree for the sensors.

Two recent studies evaluated the agreement of chemiluminescence analyzers. In a study by Borrill et al. [9], three chemiluminescence NO analyzers – Niox (Aerocrine, Sweden), Ecomedics AG analyzer CLD 88 (Ecomedics, Switzerland), and Logan model LR2149 (Logan Research, UK) were found to give repeatable but significantly different values ($P < 0.05$). Bland–Altman analysis yielded the following ratios

[mean ratio (95% limits of agreement)]; Niox:Ecomedics 1.59 (1.02–2.5), Logan:Niox 1.23 (0.72–2.13), Logan:Ecomedics 1.96 (1.09–3.57). Each analyzer was calibrated according to the manufacturer's instructions. Muller et al. [10] compared nitric oxide analyzers from three manufacturers – two NIOX, two Sievers NOA model 280, and one Ecomedics – using three calibration procedures. Calibration 1 was according to each manufacturer's instructions. Calibration 2 used only a low NO calibration gas. Calibration 3 used only a high NO calibration gas. Variability between analyzers was significantly different, and the lowest variability between analyzers was observed when the analyzers were calibrated with the same low concentration gas (calibration 2), suggesting that calibration gases and procedures are the most important factor in variability between analyzers. The analysis in the present work showed a smaller mean difference with larger 95% limits of agreement.

For the present work, it is important to note that the exact NO concentration of the calibration gas was unknown but estimated to be 75–80 ppbv NO. 77 ppbv was chosen as the value for the calibration gas mixture when determining the concentration of unknown samples with the ICOS technique because the Sievers NOA measured the calibration mixture as 76.8 ± 1.2 (SD) ppbv. If the true NO concentration in the calibration mixture is actually significantly different from this value, the ICOS measurements would remain linear but differ from values from the Sievers NOA, since the concentration is determined by comparing the unknown sample absorption feature to the absorption feature of the calibration mixture.

This work also investigated the use of an ICOS sensor for flow-independent parameter estimation. In assessing airway inflammation in chronic obstructive pulmonary disease, the flow-independent parameters, particularly F_aNO (the fraction of alveolar NO), may be more useful clinically than the standard single breath plateau NO concentration measurement. The parameter values obtained in this study were similar to reported values in severe COPD [3, 4, 26]. Flow-independent parameter estimation requires measurement of the NO plateau at high flow rates with subsequently lower NO concentrations (0.5–5 ppbv). The ICOS-based sensor was able to detect the relatively low NO concentrations at the highest flow rate (260 ml/s) using off-line breath collection with subsequent analysis in the laboratory.

5 Summary

This work reported a quantum cascade laser-based ICOS sensor operating at 1828 cm^{-1} with a minimum detectable NO concentration of 3.6 ppbv (3σ). The 3σ value is reported because this value can be reliably measured in exhaled breath. Applying wavelength modulation may improve the sensitivity by a factor of ~ 4. This work suggests that the ICOS sensor yields NO measurements that are in agreement with the Sievers nitric oxide analyzer model 280, and that the mean difference of 0.6 ppbv and limits of agreement (-3.3 ppbv and 4.3 ppbv) are comparable to those among chemiluminescence analyzers from different manufacturers and using different calibration methods. Additionally, the sensor was used in estimating flow-independent parameters, which is important in assessing inflammatory status in chronic obstructive pulmonary disease.

ACKNOWLEDGEMENTS The authors would like to thank Amir Sharafkhaneh for enrolling patients with severe chronic obstructive pulmonary disease and obtaining written informed consent at the Michael E. Debakey Veterans Affairs Medical Center (Houston, TX). David Walding provided the opportunity and assistance in operating the Sievers nitric oxide analyzer 280 at the Texas Children's Hospital (Houston, TX). The quantum cascade laser utilized in this work was provided by Alpes Lasers (Switzerland). Financial support of the work was provided by the National Aeronautics and Space Administration (NASA) Graduate Research Fellowship Program, the Texas Advanced Technology Program, the Robert Welch Foundation, and the Office of Naval Research via a subaward from Texas A&M University.

Appendix

This appendix describes the iterative algorithm for calculation of F_aNO, D_wNO, and F_wNO. The algorithm and its development were described in [24] and the equations below are derived for the flow rates used in the present study.

Let the NO plateau concentrations measured in ppbv at flows 0.0083, 0.05, and 0.25 ml/s be $F_ENO_{0.0083}$, $F_ENO_{0.05}$, and $F_ENO_{0.25}$, respectively. Then the slope (S) and intercept (I) can be calculated using geometry:

$$\begin{aligned} S &= F_aNO \\ &= (250 \times F_ENO_{0.25-50} \times F_ENO_{0.05})/(250-50) \\ &= 1.25 \times F_ENO_{0.25-0.25} \times F_ENO_{0.05}\,, \end{aligned} \tag{A.1}$$

$$\begin{aligned} I &= 50 \times F_ENO_{0.05-50} \times S \\ &= 62.5 \times (F_ENO_{0.05} - F_ENO_{0.25})\,. \end{aligned} \tag{A.2}$$

For solving for F_wNO and D_wNO, the NO plateau concentrations measured at 0.0083 and 0.05 ml/s are utilized and (1) and (5) (in Sect. 2.4) are applied for both concentrations, yielding

$$F_ENO_{0.0083} = F_WNO - \frac{I}{D_wNO} e^{-D_wNO/8.3}\,, \tag{A.3}$$

$$F_ENO_{0.05} = F_WNO - \frac{I}{D_wNO} e^{-D_wNO/50}\,. \tag{A.4}$$

By subtracting these equations and rearranging, the following equation can be obtained:

$$\frac{F_ENO_{0.0083} - F_ENO_{0.05}}{I} \times D_wNO = e^{-D_wNO/50} \times e^{-D_wNO/8.3}\,. \tag{A.5}$$

The left-hand side is a line and the right-hand side is an exponential. The solution for D_wNO is the intercept in ml/s, and F_wNO can be solved using (5) (in Sect. 2.4):

$$F_WNO_{0.05} = \frac{I}{D_wNO + F_aNO}\,. \tag{A.6}$$

For the starting point for iteration to determine D_wNO, (A.1), (A.2), and (A.6) are combined to obtain

$$D_wNO_0 = \frac{62.5 \times (F_ENO_{0.05} - F_ENO_{0.25})}{F_ENO_{0.0083} + 0.25 \times F_ENO0.05 - 1.25 \times F_ENO_{0.25}}\,. \tag{A.7}$$

For iteration, the following sequence was used:

$$D_wNO_0 = \frac{(e^{-D_wNO/50} - e^{-D_wNO/8.3}) \times 62.5 \times (F_ENO_{0.05} - F_ENO_{0.25})}{F_ENO_{0.0083} - F_ENO_{0.05}}. \quad (A.8)$$

This converges to the final value in less than 10 rounds. After D_wNO is found, F_wNO is calculated from (A.6).

REFERENCES

1 M. Zitt, Clin. Ther. **27**, 1238 (2005)
2 A.D. Smith, J.O. Cowan, K.P. Brasset, G.P. Herbison, D.R. Taylor, New Engl. J. Med. **352**, 2163 (2005)
3 C. Brindicci, B. Cosio, R. Gajdocsi, Eur. Resp. J. **20**, Suppl. 38, 174 (2002)
4 C. Brindicci, K. Ito, O. Resta, B.B. Pride, P.J. Barnes, S.A. Kharitonov, Eur. Resp. J. **26**, 52 (2005)
5 American Thoracic Society, European Respiratory Journal, Am. J. Resp. Crit. Care **171**, 912 (2005)
6 S. George, M. Hogman, S. Permutt, P. Silkoff, J. Appl. Physiol. **96**, 831 (2004)
7 N. Binding, W. Muller, P.A. Czeschinski, U. Witting, Eur. Resp. J. **16**, 499 (2000)
8 T.W. Van der Mark, E. Kort, R.J. Meijer, D.S. Postma, G.H. Koeter, Eur. Resp. J. **10**, 2120 (1997)
9 Z. Borrill, D. Clough, N. Truman, J. Morris, S. Langley, D. Singh, Resp. Med. **100**, 1392 (2006)
10 K.C. Muller, R.A. Jorres, H. Magnussen, O. Holz, Resp. Med. **99**, 631 (2005)
11 T. Hemmingsson, D. Linnarsson, R. Gambert, J. Clin. Monitor. Comput. **18**, 379 (2004)
12 H. Ganser, M. Horstjann, C.V. Suschek, P. Hering, M. Murtz, Appl. Phys. B **78**, 513 (2004)
13 C. Roller, K. Namjou, J.D. Jeffers, M. Camp, A. Mock, P.J. McCann, J. Grego, Appl. Opt. **41**, 6018 (2002)
14 D.D. Nelson, J.B. McManus, S.C. Herndon, J.H. Shorter, M.S. Zahniser, S. Blaser, L. Hvozdara, A. Muller, M. Giovannini, J. Faist, Opt. Lett. **31**, 2012 (2006)
15 A.A. Kosterev, A.L. Malinovsky, F.K. Tittel, C. Gmachl, F. Capasso, D.L. Sivco, J.N. Baillargeon, A.L. Hutchinson, A.Y. Cho, Appl. Opt. **40**, 5522 (2001)
16 L. Menzel, A.A. Kosterev, R.F. Curl, F.K. Tittel, C. Gmachl, F. Capasso, D.L. Sivco, N.J. Baillargeon, A.L. Hutchinson, A.Y. Cho, W. Urban, Appl. Phys. B **72**, 859 (2001)
17 M.L. Silva, D.M. Sonnenfroh, D.I. Rosen, M.G. Allen, A. O'Keefe, Appl. Phys. B **81**, 705 (2005)
18 Y.A. Bakhirkin, A.A. Kosterev, C. Roller, R.F. Curl, F.K. Tittel, Appl. Opt. **43**, 2257 (2004)
19 Y.A. Bakhirkin, A.A. Kosterev, R.F. Curl, F.K. Tittel, D.A. Yarekha, L. Hvozdara, M. Giovannini, J. Faist, Appl. Phys. B **82**, 149 (2006)
20 S. Blaser, D.A. Yarekha, L. Hvozdara, Y. Bonetti, A. Miller, M. Giovannini, J. Faist, Appl. Phys. Lett. **86**, 041 109 (2005)
21 L.S. Rothman, A. Barbe, D.C. Benner, L.R. Brown, C. Camy-Peyret, M.R. Carleer, K. Chance, C. Clerbaux, V. Danna, R.M. Devi, A. Fayt, J.M. Flaud, R.R. Gamache, A. Goldman, D. Jacquemart, K.W. Jucks, W.J. Lafferty, J.Y. Mandin, S.T. Massie, V. Nemtchinov, D.A. Newnham, A. Perrin, C.P. Rinsland, J. Schroeder, K.M. Smith, M.A.H. Smith, K. Tang, R.A. Toth, J. Vander Auwera, P. Varanasi, K. Yoshino, J. Quantum Spectrosc. Radiat. Transf. **82**, 5 (2003)
22 J.B. Paul, L. Larson, J.G. Anderson, Appl. Opt. **40**, 4904 (2001)
23 G. Wysocki, M. McCurdy, S. So, C. Roller, F.K. Tittel, Exhaled human breath analysis with quantum cascade laser-based gas sensors. In *Breath Analysis for Clinical Diagnosis and Therapeutic Monitoring*, ed. by A. Amann, D. Smith (World Scientific, New Jersey, 2005), pp. 75–84
24 P.E. Silkoff, P.A. McClean, A.S. Slutsky, H.G. Furlott, E. Hoffstein, S. Wakita, K.R. Chapman, J.P. Szalai, N. Zamel, Am. J. Resp. Crit. Care **155**, 260 (1997)
25 N.M. Tsoukias, S.C. George, J. Appl. Physiol. **85**, 653 (1998)
26 M. Hogman, T. Holmkvist, T. Wegener, M. Emtner, M. Andersson, H. Hedenstrom, P. Merilainen, Resp. Med. **96**, 24 (2002)
27 J.M. Bland, D.G. Altman, Statist. Methods Med. Res. **8**, 135 (1999)
28 D.G. Altman, *Practical Statistics for Medical Research* (Chapman and Hall, London, 1995), pp. 396–439